Color Channel Compensation (3C): A Fundamental Pre-Processing Step for Image Enhancement

Codruta O. Ancuti, Cosmin Ancuti, Christophe De Vleeschouwer, and Mateu Sbert

***Abstract*— This article introduces a novel solution to improve image enhancement in terms of color appearance. Our approach, called Color Channel Compensation (3C), overcomes artifacts resulting from the severely non-uniform color spectrum distribution encountered in images captured under hazy night-time conditions, underwater, or under non-uniform artificial illumination. Our solution is founded on the observation that, under such adverse conditions, the information contained in at least one color channel is close to completely lost, making the traditional enhancing techniques subject to noise and color shifting. In those cases, our pre-processing method proposes to reconstruct the lost channel based on the opponent color channel. Our algorithm subtracts a local mean from each opponent color pixel. Thereby, it partly recovers the lost color from the two colors (red-green or blue-yellow) involved in the opponent color channel. The proposed approach, whilst simple, is shown to consistently improve the outcome of conventional restoration methods. To prove the utility of our 3C operator, we provide an extensive qualitative and quantitative evaluation for white balancing, image dehazing, and underwater enhancement applications.**

***Index Terms*— Image enhancement, dehazing, color-constancy.**

I. Introduction

NOWADAYS, due to the large-scale availability of digital cameras, images are captured in a wide range of uncontrolled environments, resulting in heterogeneous acquisition quality. To mitigate this problem, numerous solutions, named image dehazing methods, have been developed to cope with the degradation caused by the atmosphere. However, as illustrated in Fig.1 and Fig. 2, for the challenging cases associated to selective spectral distribution of the illuminant, to low illumination, or to medium attenuation (e.g. caused by bad weather conditions), the existing dehazing techniques introduce unpleasing color artifacts and distortions. The contribution of our paper is twofold. First, it observes from a statistical analysis that poor visibility conditions and severe image degradation generally correspond to a strong attenuation of one of the color channels, and explains why this strong attenuation dramatically affects most existing dehazing techniques. Second, it proposes an original and effective solution to mitigate this strong color attenuation, by providing a color-compensated image that is better suited to be processed by existing dehazing solutions.

Our simple yet powerful, **Color Channel Compensation (3C)** approach builds on the observation that the vanishing of

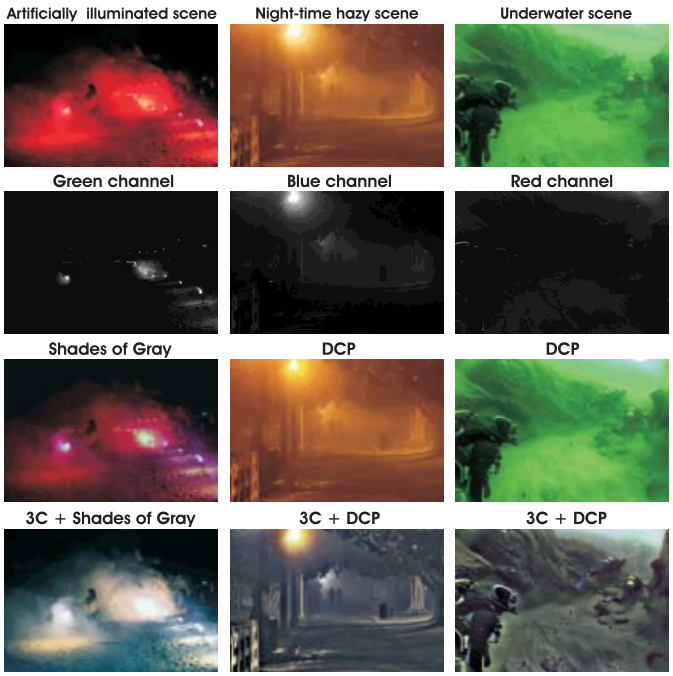

Fig. 1. Top row shows three examples of challenging images with one color channel highly attenuated (2nd row). Employing the traditional *Shades of Gray* color constancy method [1] or the well known DCP dehazing method [2] does not solve the problem (3rd row). In contrast, even if the extreme attenuation in the initial image does not allow one to recover a visually pleasant image, simply applying our 3C operator as a pre-processing step to the same techniques, results in more satisfying results in terms of color balance, thereby revealing the potential of our method. Please refer to Fig. 2 for additional comparative results.

Manuscript received April 17, 2019; revised September 17, 2019 and October 20, 2019; accepted October 23, 2019. Date of publication November 14, 2019; date of current version January 23, 2020. This work was supported in part by the Politehnica University of Timisoara, under Grant GNaC2018 ARUT and Grant 1361-01.02.2019, in part by the 2020 European Union Research and Innovation Horizon 2020 through the Grant Agreement Marie Sklodowska-Curie (TECNIOspring PLUS), under Grant 712949, in part by the Agency for the Competitiveness of the Company of the Generalitat de Catalunya, ACCIO, under Grant TECSPR17-1-0054, in part by the Belgian NSF, and in part by the Spanish Project from the Ministry of Economy and Competitivity (MINECO), under Grant TIN2016-75866-C3-3-R. The associate editor coordinating the review of this manuscript and approving it for publication was Prof. Lisimachos P. Kondi. *(Codruta O. Ancuti and Cosmin Ancuti contributed equally to this work.) (Corresponding author: Cosmin Ancuti.)*

C. O. Ancuti is with ETcTI, Universitatea Politehnica Timisoara, 300006 Timişoara, Romania.

C. Ancuti is with ETcTI, Universitatea Politehnica Timisoara, 300006 Timişoara, Romania, and also with the Institute of Informatics and Applications, University of Girona, 17004 Girona, Spain (e-mail: cosmin.ancuti@upt.ro).

C. De Vleeschouwer is with ICTEAM, Universite Catholique de Louvain, 1348 Ottignies-Louvain-la-Neuve, Belgium.

M. Sbert is with the Institute of Informatics and Applications, University of Girona, 17004 Girona, Spain.

This article has supplementary downloadable material available at http://ieeexplore.ieee.org, provided by the authors.

Digital Object Identifier 10.1109/TIP.2019.2951304

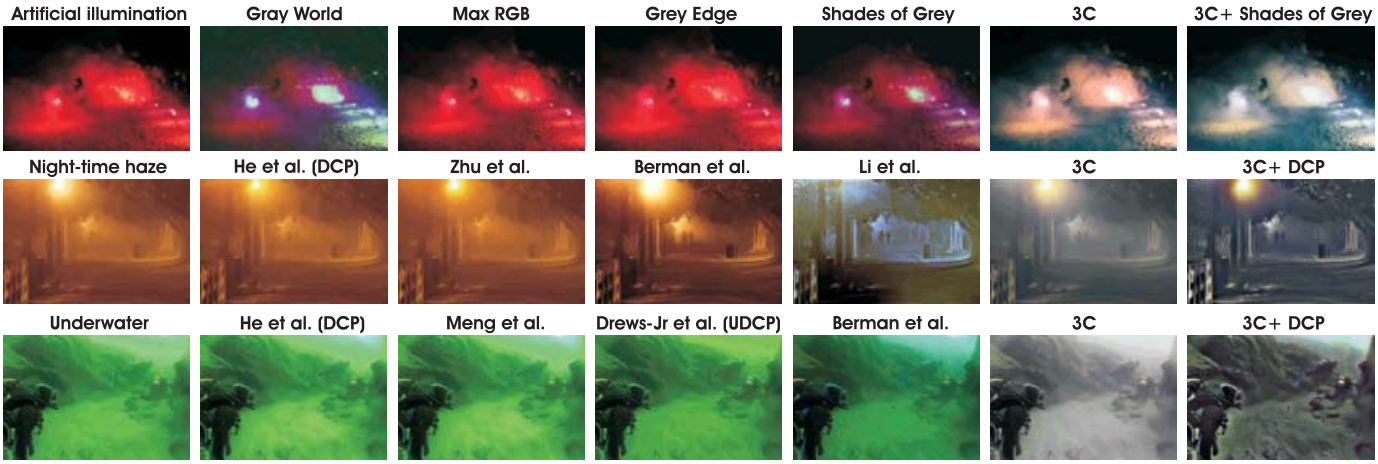

Fig. 2. **Top row** considers real extreme artificial illumination scenes. The traditional color constancy techniques (*Gray-World* [3], *Max RGB* [4], *Grey Edge* [5], and *Shades of Grey* [1]) perform poorly for this challenging scene. While our operator (3C) removes the color cast partially, *Shades of Gray* [1] pre-processed with our operator (3C) yields better results. **Middle row** shows a hazy night-time scene. Both global [2], [6] and local [7] dehazing approaches produce imperceptible improvements. Our operator applied as a pre-processing step to the same DCP dehazing technique [2] yields comparable results to those of the specialized night-time dehazing approach of Li et al. [8]. **Bottom row** shows an underwater scene. While the dehazing techniques of He et al. [2] and Meng et al. [9] but also specialized underwater methods of Drews-Jr et. al [10] and Berman et al. [11] perform poorly, our operator employed as a pre-processing step to the DCP [2] yields convincing results.

a channel tends to move (one of) the opponent color(s) away from the origin. Therefore, 3C consists in compensating for the missing channel by bringing each opponent color back towards the origin.

Our approach is motivated by a similar assumption to the one adopted by the Gray world [3], which consists in considering that the spatial average of colors in a natural scene is neutral gray. Specifically, 3C assumes that the average of each opponent color on a reasonable spatial support is close to zero. Instead of tuning R, G, and B independently, 3C works in the opponent color space, and brings back each opponent color towards zero.

When compared to previous art, our approach has been partially inspired by the recent work of [12], which demonstrates that red color channel compensation is important to restore visibility in underwater conditions. However, 3C is more general, showing robustness in a larger number of challenging cases, including underwater scenes (see Fig. 3) but also extreme visibility, as encountered in the presence of artificial sources and night-time dehazing.

To summarize, the main contributions of this paper are:

- The statistically proven observation, that, under poor illumination, or in the presence of strong and non-uniform spectral attenuation, the color information from at least one color channel might be lost for the whole scene. This complete extinction strongly penalizes existing enhancement and color-constancy solutions, which assume that all colors are preserved, while modulated by the illuminant and attenuation.
- An algorithm, named **Color Channel Compensation (3C)**, that partly restores the lost color channel from other channels, by bringing back the opponent colors towards zero-mean.
- An extensive demonstration of the consistent benefit brought by of 3C when applied as a **pre-processing step** to various image enhancement solutions for day-time and night-time image dehazing, underwater image enhancement and color constancy.

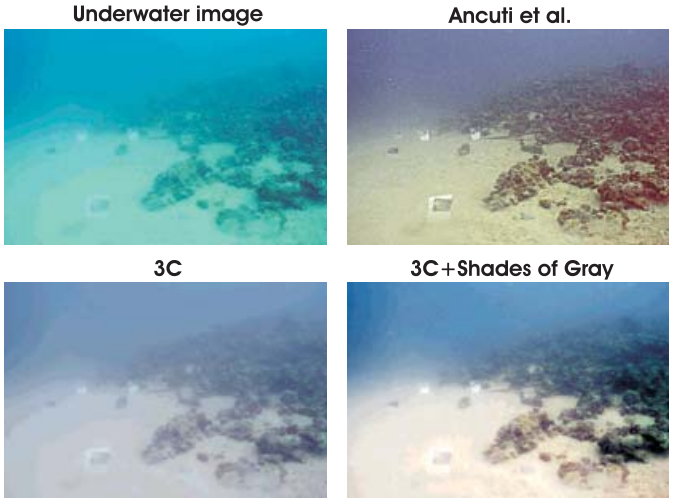

Fig. 3. The color channel correction proposed in Ancuti et al. [12] is not able to deal with noise when the image is both highly attenuated and noisy. On the other hand, 3C reduces the noise considerably. We observe that the banding effect that is present in the original image has disappeared in the image provide by Ancuti et al. [12]. This is because [12] includes a multiscale image enhancement step that is not present in 3C.

II. Related Work

Most image dehazing solutions resort to the optical model of Koschmieder [13]. This model states that the light intensity $\mathcal{I}(x)$ at each image coordinate x results from two main additive components - direct transmission $\mathcal{D}(x)$ and airlight $\mathcal{A}(x)$:

$$\mathcal{I}(x) = \mathcal{D}(x) + \mathcal{A}(x) = \mathcal{J}(x)\ T\ (x) + A_{\infty}\ \ [1 - T\ (x)] \quad (1)$$

where $\mathcal{J}(x)$ is the scene radiance, $T(x)$ is the transmission along the cone of vision (decreasing exponentially with the depth of the scene), and A_{∞} is the atmospheric intensity,

a color vector resulting from environmental illumination. To estimate the transmission, many of the existing dehazing solutions build on the dark channel prior (DCP) [2]. Initially proposed for outdoor dehazing, DCP was introduced based on the statistical observation that all regions in a natural scenes contain some pixels that have very low intensities in at least one color channel. It consequently defines regions of small transmission as the ones with large minimal values of colors.

Day-time single image dehazing techniques [14]–[17] build upon the simplified Koschmieder light transmission model [13] and on some prior knowledge, such as Dark Channel Prior (DCP) [2], saturation and intensity, [6] and color channels distribution (e.g., color-lines [16] and haze-line [7]). In contrast, image dehazing based on fusion strategies [18] have the advantage of not requiring explicit estimation of the transmission [19], [20] and offer more robustness to the airlight changes induced by artificial lighting [21]. Recently, several learning-based methods [22]–[24] have also demonstrated their effectiveness for haze removal. As attested by our experimental section, all methods however suffer in presence of severe attenuation.

Night-time dehazing deals with scenes that include multiple light sources, which tend to generate glowing artifacts. Several dedicated night-time dehazing methods [8], [21], [25], [26] have been introduced to account for spatially non-uniform illumination. Recently, a few more solutions have been proposed to deal with haze under night-time conditions [8], [21], [26]. While our 3C operator is not an image dehazing approach, we prove that it constitutes a valuable pre-processing step to enhance both those daytime and night-time dehazing methods.

Underwater image enhancement. Most recent underwater enhancing solutions [10], [27]–[31] have been inspired by outdoor dehazing strategies, assuming that the light propagation is reasonably well approximated by the Koschmieder's model [13]. Dark Channel Prior (DCP) [2] is the foundation for many underwater strategies [10], [32], as well as for outdoor dehazing. In the presence of extreme attenuation of the red channel, Ancuti *et al.* [12] compensate for the vanishing of red based on the green channel. Our 3C operator can be seen as a generalization of [12] that is able to deal with the vanishing of an arbitrary color channel (in turbid water the blue channel is more attenuated than the red one, see Fig. 3), independently of whether this vanishing is due to attenuation during transmission (underwater or severe haze) or to a missing spectral components in the illuminant (night-time artificial lighting).

Color constancy or white balance techniques aim at making imaged colors invariant to the scene's illumination, but assume that all channels are present (whilst differently affected by lighting) in the captured image. Therefore, color constancy infers and compensates for the undesirable color casts induced by the illuminant. Being mathematically ill-posed, it remains a challenging problem. The existing methods [33] make various assumptions regarding some regularity in the colors distribution of natural objects under neutral illumination conditions. Early approaches [1], [3]–[5] assume that colors are equally represented at the scene level. For instance in the Gray World [3] the illuminant color is identified by simply estimating the mean of each color channel in the initial image. Hence, it considers that the average reflectance of a scene is in general achromatic. The *Shades-of-Grey* color constancy method was introduced by Finlayson and Trezzi [1] and builds on the observation that the *Max-RGB* [4] and Gray-World methods are two instantiations of the Minkowski p-norm applied to the native pixels, respectively with $p = +inf$ and $p = 1$. *Shades-of-Grey* extends the process to arbitrary p values. The best results are obtained for $p = 6$. As stated above, our 3C operator relies on a similar assumption, but implements it in the opponent color space to compensate for the vanishing of a full color band.

Another class of color constancy techniques uses various strategies to learn the color distribution of a training data set [34]–[37]. More recently, color constancy methods have been proposed to deal with multiple illumination sources [38]–[40].

In contrast, our 3C operator focuses on the recovery of the missing information and compensates for the loss of one particular color channel, e.g., due to a selective illumination spectrum or strong attenuation of a subset of wavelengths. Such cases are frequent in scenes with high selective attenuation such as underwater, where the perception of certain colors is influenced by the red channel attenuation (in water red disappears first, then orange, yellow, and so on). Similarly, in yellowish muddy turbid waters, the blue channel is highly attenuated. The loss of a color channel is also common when artificial illumination introduces a high degree of color distortion due to a selective lighting spectrum. Basically, our 3C operator **does not provide an alternative to existing color constancy techniques, but rather complement them to perform better on various extreme cases** (see Fig. 10). Like most color constancy approaches, our 3C operator neglects the colorimetric mapping errors induced by the sensor-specific color space transform [41] and focuses on the prominent color degradation caused by a severely biased illumination or a strong wavelength-specific transmission attenuation.

Opponent color spaces have been introduced to reflect the fact that the human visual system interprets information about color by processing signals from photoreceptor cells antagonistically. An opponent color space builds on the assumption that the visual system manipulates differences between the responses of the three types of cones (Blue/Green/Red wavelengths), rather than each type of cone's individual response. The opponent color theory considers that there are two chromatic opponent channels (red versus green, blue versus yellow) and one achromatic channel (black versus white). It accounts for perceptual dependencies between color bands, so as to model color perception phenomena that cannot be explained by processing the RGB channels independently, such as the fact that humans do not perceive reddish-greens and bluish-yellows. Our paper reveals that an opponent color space allows to naturally reconstruct a missing channel when necessary. Specifically, it shows that subtracting (a fraction of) local means to opponent colors helps in compensating the missing green, blue or red color with respect to their opponent counterpart

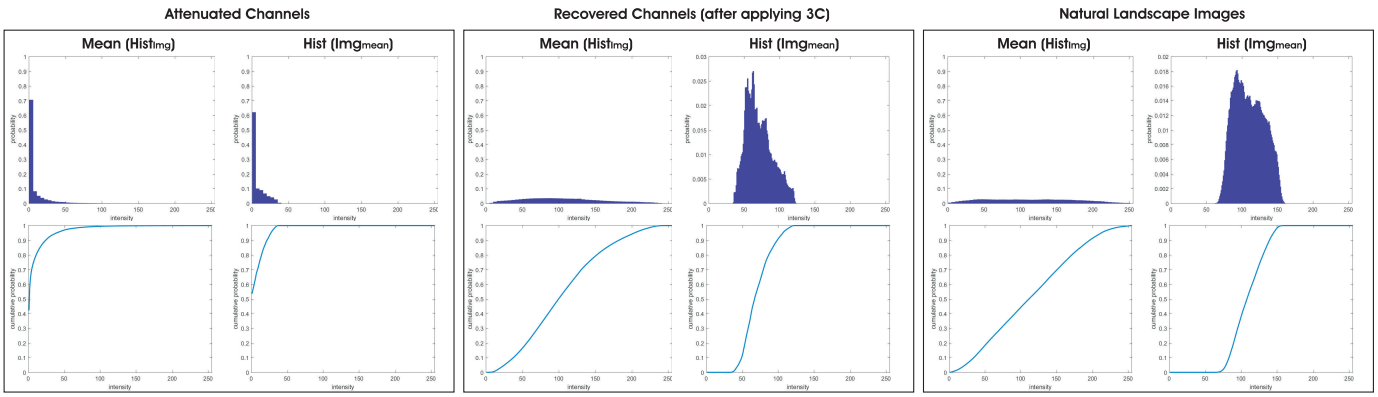

Fig. 4. We present the statistics of the attenuated color channel of a set of $+$**2000** real images before and after applying 3C. The images have been captured in challenging conditions (underwater, night-time haze and artificial illumination), and the conventional DCP implementation appears to be ineffective in restoring them. On those images, we have observed that one color channel (not always the same) is severely attenuated. From left to right are shown the histograms of the attenuated channel in each image, the histograms of restored image channels (after pre-processing them with our operator 3C), and the histograms of (1000+) natural landscapes images. $Mean(Hist_{Img})$ presents the mean of the histogram vectors while the $Hist(Img_{Mean})$ presents the distribution of the mean of each image. For a better understanding the bottom row presents the cumulative distribution functions (CDF). As can be seen after applying our operator 3C results in statistical distributions that are closer to the one of natural images.

III. Color Channels Compensation (3C)

A. 3C Motivation: Strong Color Channel Attenuation

Our Color Channels Compensation (3C) operator is motivated by the key observation that images obtained under extreme visibility conditions (underwater, night-time haze, and artificial illumination) present stronger losses in one channel than in others.

To make this observation, we gathered a large database of images (2000+ images) taken under challenging conditions (underwater, night-time haze and artificial illumination). Since most of the dehazing solutions are based on using DCP to invert the optical model, we selected primarily images that were not effectively enhanced by the conventional DCP implementation [2]. After careful analysis of these images and their color channels statistics, we observed that all of them had a common characteristic: one color channel was made of large areas of zero values (see the peak in the origin in Fig. 4, where 60% of the pixels have 0 intensity, 90% of the pixels have lower than 25 intensity, and 98% of the pixels exhibit intensities below 40) or lacked scene-relevant spatial distribution of intensity.

This loss of information is either the consequence of the illumination characteristics (some range of wavelengths is missing from the light spectrum) or due to the characteristics of the medium: selective attenuation, scattering phenomena (Rayleigh). In hazy night-time images, for instance, the yellowish illuminant generates images with highly attenuated blue channels, due to the multiplication between scene reflectance and the illuminant. In clean water, the wavelengths are attenuated selectively. Radiations with lower frequency are more absorbed, which implies that the red intensity is attenuated usually after 5-6 m, the orange after 7-8 m, yellow after 10-15 m, and the green around 21 m. Hence, images taken at greater depths will present a blue (blue-green) appearance. In aerial medium, the atmospheric scattering (Rayleight scattering) also depends on the wavelength. Shorter wavelengths (corresponding to blue color) are more scattered than longer ones. Rayleigh scattering is easily noticeable since it causes the blue sky during the daytime.

Now that we have observed that the most challenging cases are characterized by the extinction of one color, due to attenuation or selective lighting spectrum, we better understand why conventional dehazing methods generally fail in those cases: the unbalanced attenuation induces color shifting; the dark channel prior, which associates a small minimal color value to a good transmission, systematically fails in estimating the transmission; and conventional enhancement methods, which attempt to reconstruct a pleasant image by resorting to some kind of histogram stretching (often guided by the inversion of an approximated light transmission model) for each channel, tend to amplify noise when the information is missing in one channel.

To circumvent the channel extinction issue, we propose to compensate for it. Therefore, we observe from our dataset that the severe color attenuation affects primarily one of the opposite colors in opponent color space. In other words, images that are subject to severe color artifacts generally look either blue, yellow, red, or green.

Hence, working in the CIE$L^*a^*b^*$ [42] opponent space should facilitate the compensation of strong color shifts induced by common attenuation/lighting spectral distribution. For example, in greenish pictures, since the loss of red induces an a^* channel shift in favor of the green color, this loss could be offset/mitigated by bringing back the a^* channel towards mean zero values or, equivalently (see Section III.B), by adding a fraction of the green signal to the red channel, as recommended in [12]. The same holds for the b^* channel when dealing with blueish (loss of yellow, i.e., red+green) and yellowish (loss of blue) pictures.

In other words, because the color opponent space combines the spectral components of color, the correlation encountered in natural scenes between the R, G, and B components is partly reflected in the statistical distribution of the opponent colors, making it possible to recover one particular missing R, G, or B channel by restoring the statistical properties expected

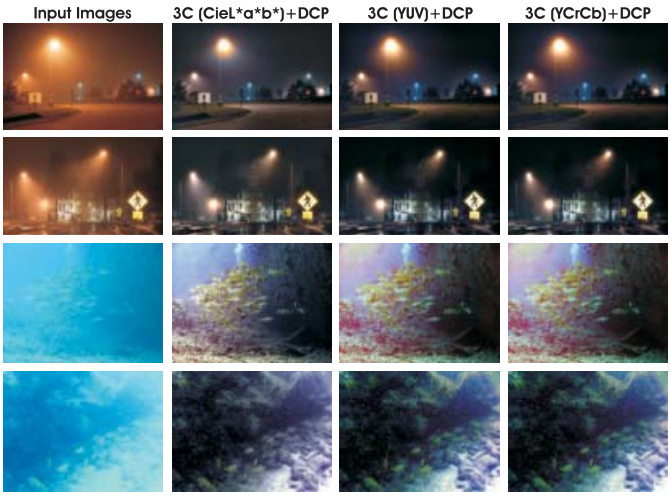

Fig. 5. Applying 3C in different color-opponent spaces, yields quite similar results.

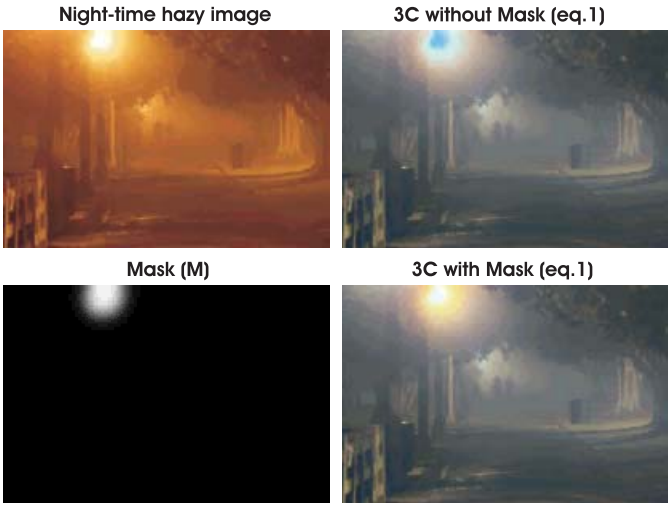

Fig. 6. The influence of the mask (M) defined in Equation 2. If the mask is not defined, the regions close to the illumination sources are affected by color shifting.

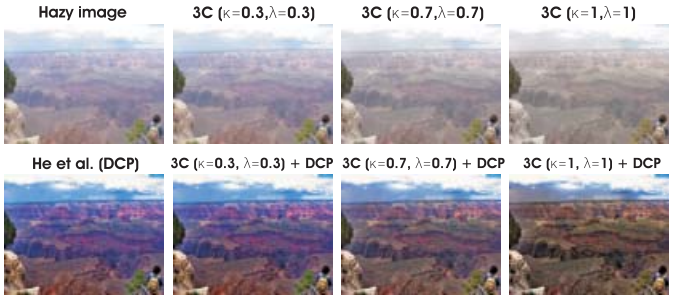

Fig. 7. **The impact of κ and λ parameters.** In Equation 2 the parameters κ and λ define the level of compensation. The compensation increases proportionally to the value of the κ and λ parameters. Setting $\kappa = \lambda = 0.7$ generally results in the most pleasant images.

TABLE I

AVERAGE CIEDE00 VALUE FOR COMPUTED FOR 5 HAZY IMAGES OF THE O-HAZE DATASET PROCESSED WITH 3C OPERATOR BY VARYING THE λ AND κ PARAMETERS (THE SMALLER THE CIEDEOO THE BETTER)

κ \ λ	**0**	**0.3**	**0.5**	**0.6**	**0.7**	**1**	**1.2**
0	16.674	16.6745	16.7196	16.826	16.9937	17.2145	17.4913
0.3	14.9984	15.0134	15.072	15.1772	15.3446	15.5709	15.8677
0.5	13.5233	13.4668	13.4674	13.5368	13.6832	13.9109	14.2209
0.6	12.4331	12.2178	12.0826	12.0368	12.1015	12.2976	12.622
0.7	12.4727	12.0901	11.7487	11.4868	**11.3656**	11.4277	11.702
1	13.9044	13.5236	13.1821	12.893	12.7069	12.6675	12.8162
1.2	15.991	15.7299	15.5014	15.3202	15.204	15.206	15.368

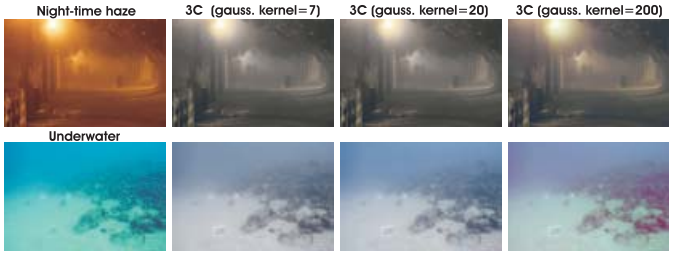

Fig. 8. **Gaussian filter size impact.** When the size of the Gaussian kernel is too small, the image losses the chromatic information. For a too-large kernel size, the compensation is suboptimal/incomplete.

from the opponent colors. In particular, we have observed that, when one of the R, G, and B component is severely attenuated, it can be recovered by pushing the opponent colors towards a zero local mean. We have tested other color-opponent spaces and the results are quite similar (see Fig. 5).

B. Color Channel Compensation

Our enhancement pre-processing method assumes that the mean of the each opponent channel is zero (neutral color) when a sufficiently large scene is considered. Under this assumption, which sounds like a transposition of the Gray World [3] assumption to the opponent color space, a simple way to mitigate the color shifts induced by severe spectral power discrepancies induced by a biased illuminant or a severe attenuation consists in subtracting the mean of each opponent color channel, as averaged on the whole scene, from the channel itself. In practice however, the level of color attenuation (and thus color shift) may vary spatially. Therefore, a local mean, estimated by a Gaussian filter with large spatial support, is subtracted from each opponent channel. Formally, the compensated opponent color channels I^c_{a*} and I^c_{b*} are computed in every pixel x as:

$$\begin{aligned} I^c_{a*}(x) &= I_{a*}(x) - \kappa \cdot M(x) \cdot GI_{a*}(x) \\ I^c_{b*}(x) &= I_{b*}(x) - \lambda \cdot M(x) \cdot GI_{b*}(x) \end{aligned} \tag{2}$$

where I_{a*}, I_{b*} are the initial color opponent channels and GI_{a*} and GI_{b*} represent their Gaussian filtered versions. The parameters κ and λ adjust the level of correction for the two opponent channels. As illustrated by Fig.7, κ and λ should be chosen reasonably large to mitigate the color shift induced by the excessively attenuated color channel. W Based on extensive qualitative and quantitative (see Table I) testing on hazy images (day/night/underwater), we came to the conclusion that, in general, setting the κ and λ parameters around 0.7 results in visually pleasant outputs. However, in underwater, since the attenuation is much higher and selective

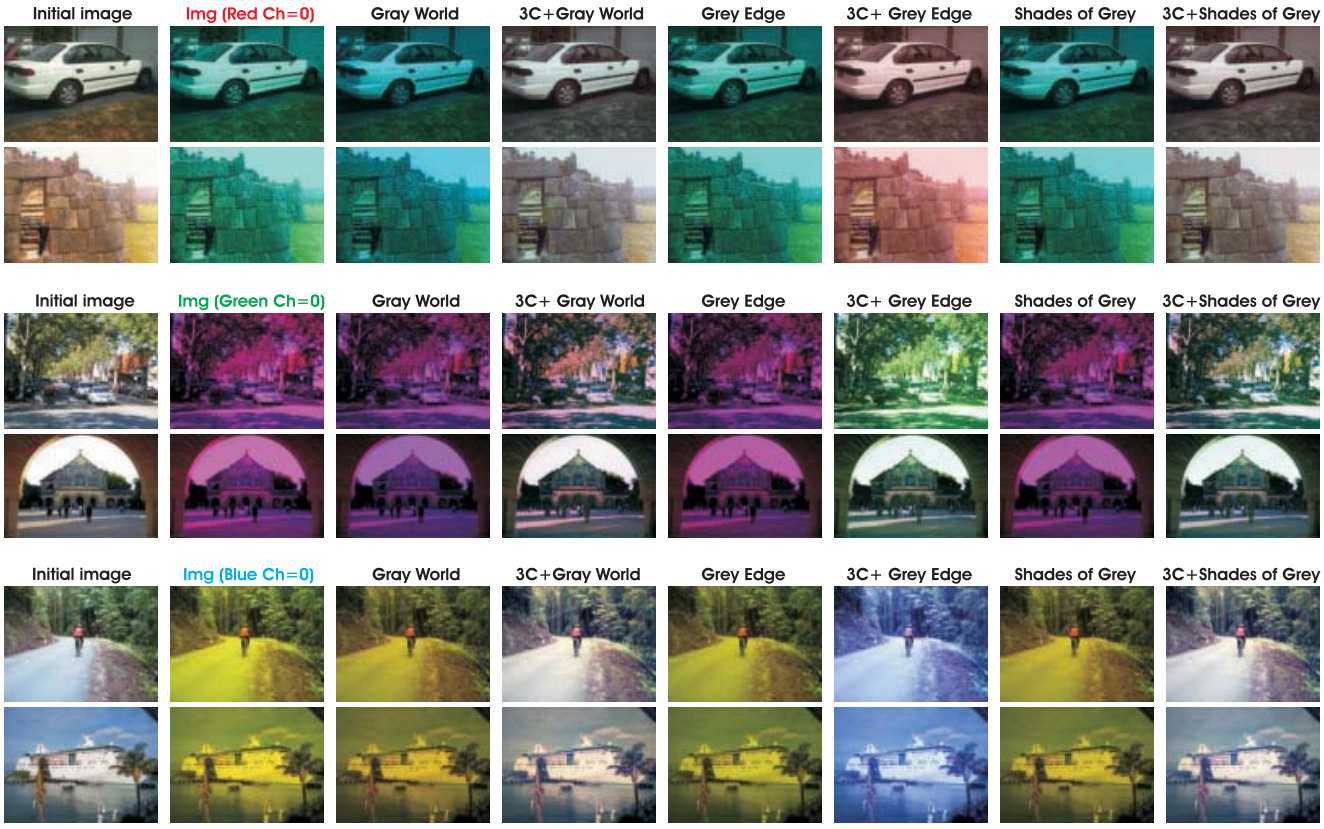

Fig. 9. **Synthetic images.** The first column shows the initial color image (from the *Stanford Background Dataset*) and the second column shows the synthetic images obtained when one of the color channels (e.g., Red, Blue and Green) has been completely removed (all its values are set to 0). The next columns show the results obtained with two traditional color constancy techniques, *Gray World* **[1]** and *Max RGB*, **[2]** and the results when our operator (3C) is applied as a pre-processing step to those methods. The quantitative evaluation over the entire dataset (700+ images) is provided in Table II.

(in terms of wavelength), it becomes relevant to increase the correction for the red-green channel (because red is subject to higher attenuation in underwater medium), while keeping the generally recommended level of compensation for the yellow-blue channel. As a consequence, κ is set to 1, while λ is kept to 0.7 in underwater. The mask M is a refinement that has been introduced to maintain significant illumination in light source locations. For a pixel location, the mask value is set to zero when $mean(r, g, b) > 0.85$ and to 1 elsewhere. To avoid artifacts (see Fig. 8), the mask is smoothed with a simple Gaussian with a medium kernel size (default size is set to 20).

Interestingly, Equation 2 appears to be an extension, but also an elegant formulation, of the red channel compensation introduced by Ancuti et al. in [12], where the compensated red channel I_r^c at every pixel location (x) has been defined as:

$$I_r^c(x) = I_r(x) + \alpha \cdot (\bar{I}_g - \bar{I}_r) \cdot (1 - I_r(x)) \cdot I_g(x) \quad (3)$$

with I_r, I_g being the red and green color channels of the initial image I, each channel being in the range [0, 1], after normalization by the upper limits of their dynamic ranges; and $\bar{I}_r$ and $\bar{I}_g$ denoting the average of those channels over the whole image. α is a constant parameter. Despite its effectiveness for underwater scenes, Equation 3 has two main limitations: first, if the red channel is entirely attenuated, then, based on Equation 3, the green channel values are transferred entirely to the red channel and will give the restored scene unwanted yellowish appearance. Secondly, this solution has been tailored for underwater scenes and is not applicable to any color attenuation than the red. In contrast, our solution is general and can be used to solve severe attenuation conditions for turbid water or night-time scenes, where the blue channel may be significantly attenuated due to absorption by organic matter or the spectral power distribution of the artificial light spectrum.

To reveal the link between Equation 3 and our method in Equation 2, we consider the red component to be severely attenuated ($I_r \sim 0$), which is the use case of interest in [12], in Equation 2. In that case, Equation 3 can be approximated as:

$$I_r^c(x) = I_r(x) + \alpha \cdot \bar{I}_g \cdot I_g(x) \quad (4)$$

By approximating the opponent color channel I_{a*} by $\gamma \cdot (I_g - I_r)$, the first line of Equation 2 becomes, with mask M set to 1:

$$I_g^c(x) - I_r^c(x) = I_g(x) - I_r(x) - \gamma\, G\left\{I_g(x) - I_r(x)\right\} \quad (5)$$

with $\gamma = \alpha \cdot \bar{I}_g$. Given $I_g^c(x) = I_g(x)$ in [12] and $I_r \ll I_g$ (since $I_r \sim 0$), Equation 5 appears to be identical to Equation 4, up to the Gaussian filtering applied to I_g $(G\left\{I_g(x)\right\})$ in Equation 5. Hence, we conclude that

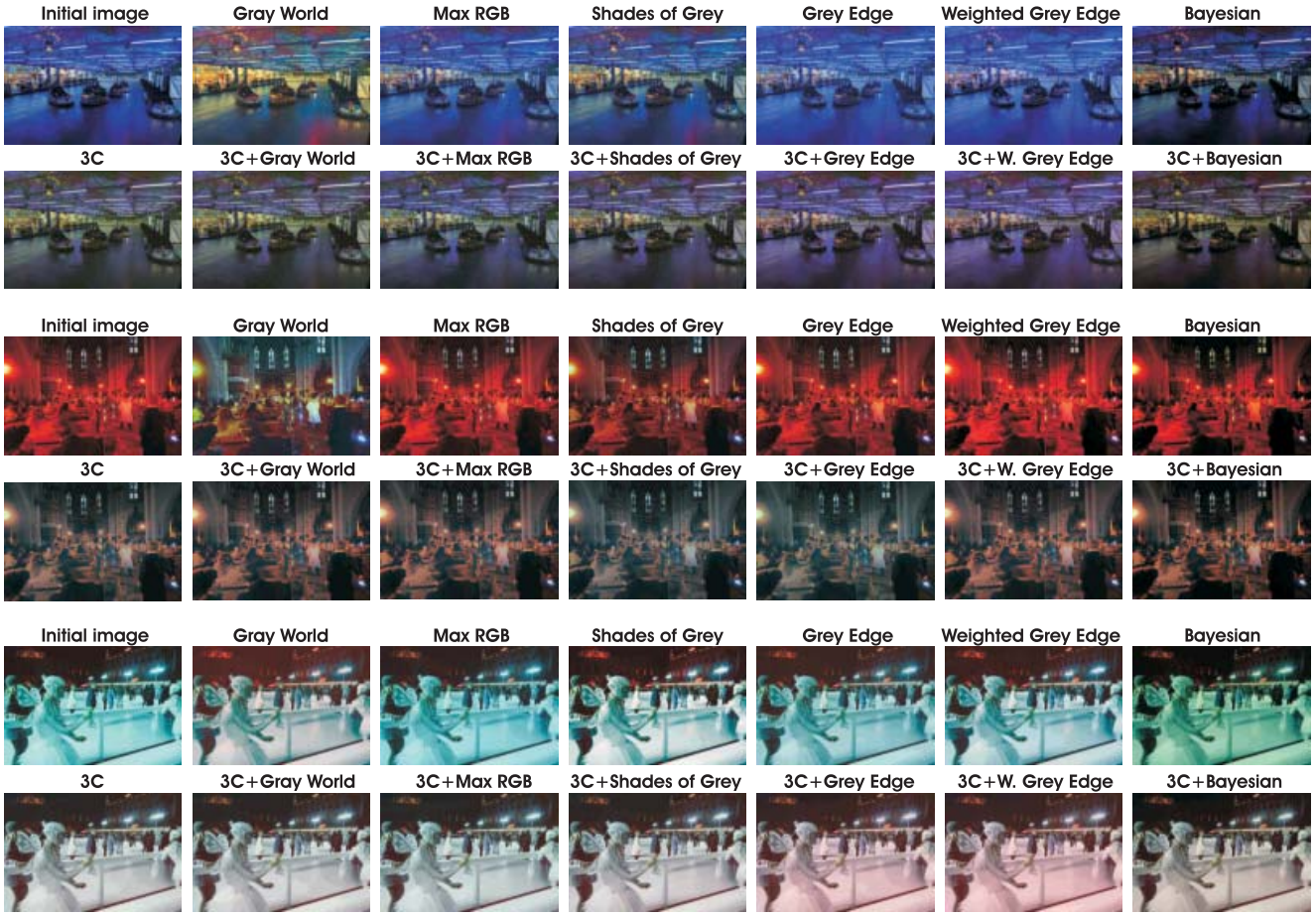

Fig. 10. **Enhancing artificially illuminated (real) scenes.** We present three examples of real images captured in presence of artificial illumination. For each scene, the top (bottom) row shows the results produced by several traditional color constancy methods, without (with) our 3C pre-processing operator. Color constancy methods include: *max RGB* [4], *Gray Word* [3], *Shades of Grey* [1], *Gray Edge* [5], *Weighted Gray Edge*, [44] and *Bayesian Color Constancy* [34]. It is easy to see that our operator, 3C, applied as a pre-processing step to the color constancy methods, yields better results. For more results the reader is referred to the supplementary material.

Equation 2 is equivalent to Equation 3 in the use case recommended by [12] (red attenuation).

IV. Experimental Results and Discussions

A. 3C for Color Constancy

Although color constancy has been ignored by many image dehazing and underwater image enhancement methods, [19] and [12] observed that, due to the airlight estimation ambiguity, image dehazing algorithms generate images that are visually more pleasant when they are applied to inputs that have been pre-processed with a color constancy method.

Traditional color constancy, however, appears to be unable to deal with extreme cases (see Fig. 10). This is because color constancy adjusts the contrast independently for each color channel. Hence, when a channel is missing, this operation is prone to introduce artifacts or have no influence at all, thereby preserving a prominent color shifting.

To demonstrate the utility of 3C for such cases (images with one color channel highly attenuated), we first considered a dataset of outdoor natural images, including the *Stanford Background Dataset* [43], and emulate strong attenuation conditions by zeroing one color channel at a time, as in the example shown in Fig. 9. We applied several traditional color constancy techniques to the set of artificially attenuated images, namely, : the white-patch, *max RGB* algorithm [4], the *Gray World* [3], *Shades of Grey*, [1] and *Gray Edge* [5].

Table II relies on the CIEde00 metric [45] to compare the results of these color constancy techniques when applied with and without 3C pre-processing. CIEde00 generates values in the range [0,100], with smaller values indicating small color difference to the ground truth. For completeness, in Table II we also provide the PSNR results for the entire synthetically generated *Stanford Background Dataset*.

As a second component of our validation, Fig. 10 shows three examples of artificially illuminated real scenes. For each scene, the top row shows the results produced by several traditional color constancy methods: *max RGB* [4], *Gray Word* [3], *Shades of Grey* [1], *Gray Edge* [5], *Weighted Gray Edge*, [44] and *Bayesian Color Constancy* [34]. It can be observed in the second row that applying our 3C operator as a pre-processing step to the same color constancy methods, yields better results. For more visual results the reader is referred to the supplementary material.

TABLE II

QUANTITATIVE EVALUATION: INPUT IMAGES ARE OBTAINED BY SETTING TO ZERO A WHOLE CHANNEL IN IMAGES OF THE STANFORD BACKGROUND DATASET [43] (700+ IMAGES). PSNR AND CIEDE00 QUALITY OF IMAGES RECONSTRUCTED BY A NUMBER OF CONVENTIONAL METHODS, WITH AND WITHOUT 3C PRE-PROCESSING. A NATURAL IMAGE AND ITS SYNTHETIC VERSIONS ARE SHOWN IN FIG. 9. MORE EXAMPLES ARE PROVIDED ON THE PROJECT PAGE HTTPS://SITES.UCLOUVAIN.BE/ISPGROUP/RESEARCH/3C

	Initial imgages		Gray World		max RGB		Grey Edge		Shades of Grey	
	PSNR	**CIEde00**	**PSNR**	**CIEde00**	**PSNR**	**CIEde00**	**PSNR**	**CIEde00**	**PSNR**	**CIEde00**
Imgs (Red ch. removed)	15.976	20.936	12.743	23.197	12.858	22.518	12.987	22.561	12.931	22.831
3C on Imgs (Red ch. removed)	23.872	11.541	23.845	11.548	24.040	13.099	24.503	18.636	23.851	12.000
Imgs (Green ch. removed)	9.972	33.624	8.938	36.578	8.940	36.014	8.966	35.944	8.969	36.169
3C on Imgs (Green ch. removed)	11.396	25.520	11.474	25.110	12.418	24.178	13.233	24.758	11.815	24.276
Imgs (Blue ch. removed)	24.322	23.999	16.619	24.163	16.653	23.977	16.719	24.013	16.617	24.077
3C on Imgs (Blue ch. removed)	32.465	11.755	31.843	11.697	29.200	13.756	27.534	23.181	29.812	12.356

TABLE III

QUANTITATIVE RESULTS FOR THE GEHLER-SHI COLOR CONSTANCY DATASET. SUMMARIZING ANGULAR ERRORS OF THE TRADITIONAL COLOR CONSTANCY METHODS OF GRAY WORD (GW) [3], MAX RGB WHITE PATCH (WP) [4], GRAY EDGE (GE) [5] AND SHADES OF GRAY (SOG) [1]. APPLYING 3C AS A PRE-PROCESSING STEP TO THESE TRADITIONAL METHODS IMPROVES THEIR ORIGINAL PERFORMANCE, LEADING TO RESULTS THAT ARE COMPARABLE WITH THE LEARNING-BASED TECHNIQUES OF [34] (BAYESIAN), [39] (NIS) AND [35] (MLS)

	GW [3]	**3C+GW**	**WP** [4]	**3C+ WP**	**GE** [5]	**3C+GE**	**SoG** [1]	**3C+SoG**	**Bayesian** [34]	**NIS** [39]	**MLS** [35]
Mean	6.34	4.94	7.53	4.81	5.17	4.87	4.91	4.67	4.82	4.19	4.16
Median	6.25	4.01	5.64	3.77	4.43	3.9	4.02	3.38	3.46	3.13	3.3

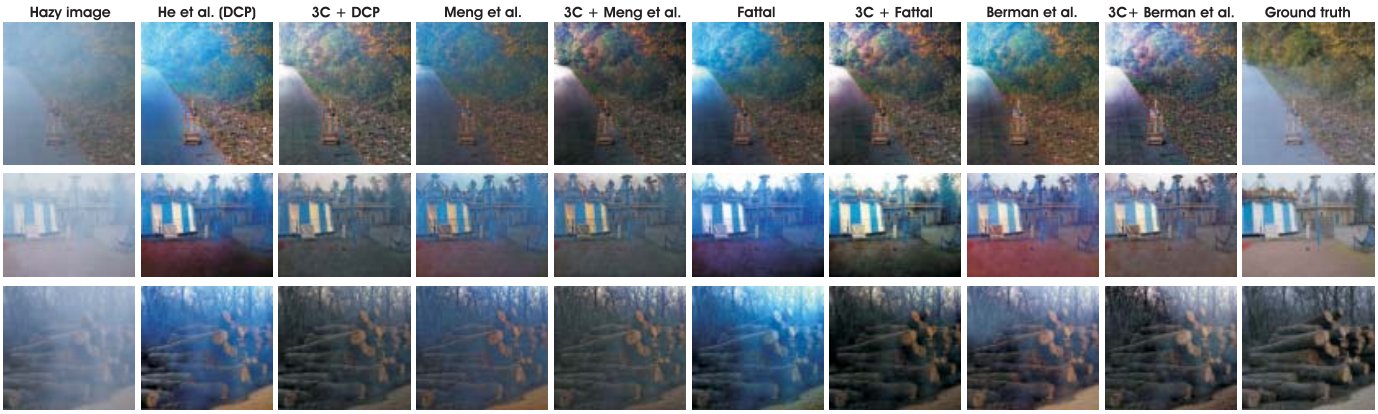

Fig. 11. **Day-time dehazing.** Three images of the O-Haze [46] dataset are processed by four specialized single-image dehazing techniques, namely He et al. [2], Meng et al. [9], Fattal [16], and Berman et al. [7]. As demonstrated also quantitatively in Table IV, applying 3C as a pre-processing step to those dehazing methods, yields better results. The last column shows the ground-truth images.

Table III provides quantitative results also for the well-known Gehler-Shi color constancy dataset [34]. It demonstrates that 3C improves traditional color constancy techniques significantly, yielding results that are competitive with learning-based color constancy methods.

B. 3C for Image Enhancement

This sub-section shows the utility of our 3C operator in the context of image enhancement. It considers several challenging applications, such as day-time and night-time image dehazing and underwater image enhancement.

Image dehazing generally resorts to the inversion of the optical model of Koschmieder [13], which requires *transmission* and *airlight* estimation. The estimation of transmission is most often performed based on the dark channel prior (DCP), [2] which estimates the attenuation proportionally to the smallest color value, and is thus severely misled when a full channel has been lost. The airlight is estimated either globally or locally depending on the assumptions about the illumination sources (airlight is assumed to be uniform for hazy day-time images and non-uniform for the hazy night-time images or underwater images). In those methods, the airlight estimation is tightly connected to the transmission estimation, since airlight is estimated as observed at the point with smallest transmission.

Regarding the validation of our 3C solution, we first consider the recent outdoor dataset O-Haze, [46] which contains 45 pairs of real hazy and corresponding haze-free ground-truth images. Fig. 11 shows three images and the results generated by four specialized single-image dehazing techniques [2], [7], [9], [16]. We observed that the results of the same dehazing techniques looks better when the images are pre-processed by our 3C operator. Table IV presents the PSNR and CIEde00 values averaged over the entire O-Haze dataset and confirms quantitatively our visual observation. More visual comparisons are provided in the supplementary material.

Night-time dehazing is more challenging since it involves artificial light sources, which tend to introduce additional

TABLE IV

QUANTITATIVE EVALUATION OF DAY-TIME DEHAZING. THIS TABLE PRESENTS PSNR AND CIEDE00 AVERAGED OVER THE ENTIRE O-HAZE [46] DATASET, WITH AND WITHOUT 3C AS A PRE-PROCESSING STEP. THREE IMAGES AND CORRESPONDING DEHAZED IMAGES OF HE ET AL. (DCP) [2], MENG ET AL. [9], FATTAL [16] AND BERMAN ET AL. [7] ARE SHOWN IN FIG. 11

	DCP [2]	**3C+ DCP**	**Meng** [9]	**3C+ Meng**	**Fattal** [16]	**3C+Fattal**	**Berman** [7]	**3C+Berman**
CIEde00	20.745	14.255	16.968	15.232	19.854	16.656	17.088	15.148
PSNR	16.586	17.755	17.443	17.676	15.639	16.136	16.610	16.953

Fig. 12. **Night-time dehazing.** Qualitative comparison of the results generated by the global dehazing techniques of He et al. [2] and Meng et al. [9], the local dehazing approaches of Ancuti et al. [21] and Berman et al. [7], and the results of our operator (3C) applied as a pre-processing step to *Shades of Gray* [1] color constancy method and He et al. (DCP) [2] dehazing method.

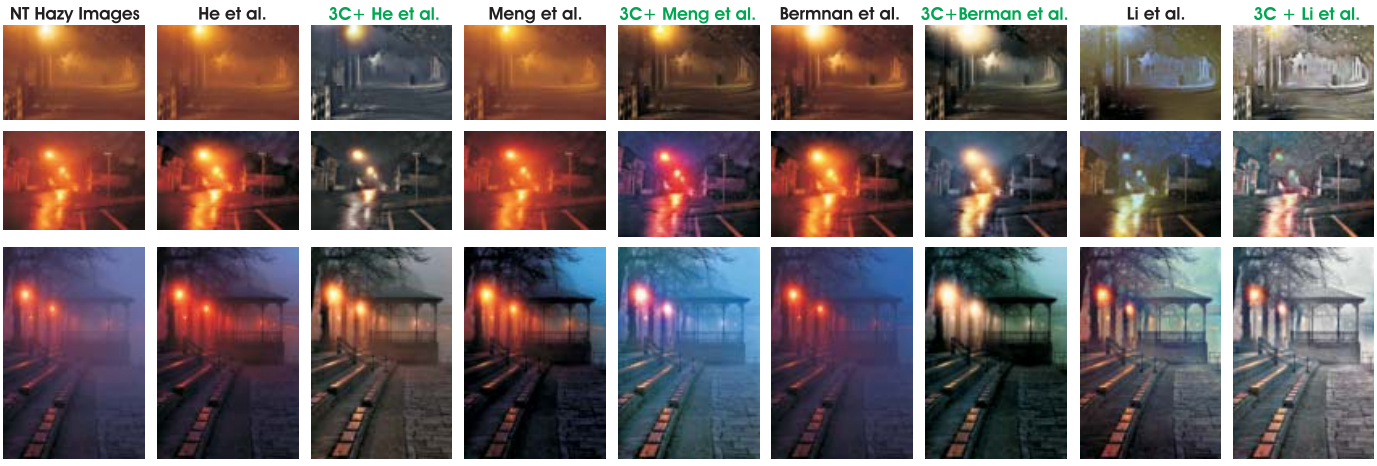

Fig. 13. **Night-time dehazing.** Our operator (3C) applied as a pre-processing step significantly improves the effectiveness of day-time dehazing techniques (He et al. [2], Meng et al. [9], Berman et al. [7]) as well for hazy night-time scenes. Interestingly, our 3C operator also improves the specialized night-time dehazing technique of Li et al. [8] considerably.

color shifting. We consider the 130+ images of the night-time dehazing dataset introduced by Li *et al.* [8] (see Fig. 2 and also the supplementary material). Since for night-time dehazing there is no specialized quality metrics, we provide qualitative comparative results but also a perceptual evaluation based on a user study. Fig. 12 presents two hazy night-time images. As can be seen, the results of *Shades of Gray* [1] and DCP on images pre-processed by our operator are comparable and even better than the results yielded by the local dehazing techniques of Ancuti *et al.* [21] and Berman *et al.* [7]. Moreover, as shown in Fig. 13, our 3C operator applied as a pre-processing step makes the day-time dehazing techniques (He *et al.* [2], Meng *et al.* [9], Berman *et al.* [7]) effective for hazy night-time scenes, as well. In addition, our operator 3C improves the specialized night-time dehazing technique of Li *et al.* [8] considerably.

In the user study we compared the techniques of He *et al.* [2], Meng *et al.* [9], Berman *et al.* [7] and Li *et al.* [8] and the same techniques pre-processed by our operator 3C

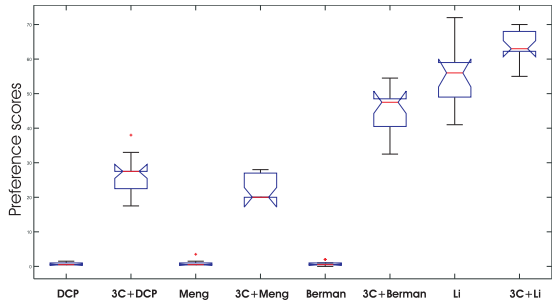

Fig. 14. **Statistical analysis of the user study for night time dehazing**. 15 users were asked to rank 8 results in decreasing order of visual quality. The best four results have been scored to, 80%, 60%, 40% and 20%, respectively, while the rest of them have been classified as acceptable (scored with 10%) or not acceptable (not scored). We interpret the results statistically using analysis of variance (ANOVA) [47].

(see Figure 13). The group consisted of 15 volunteers ages 20-45, with normal or corrected-to-normal visual acuity and no issues related to the perception of colors.

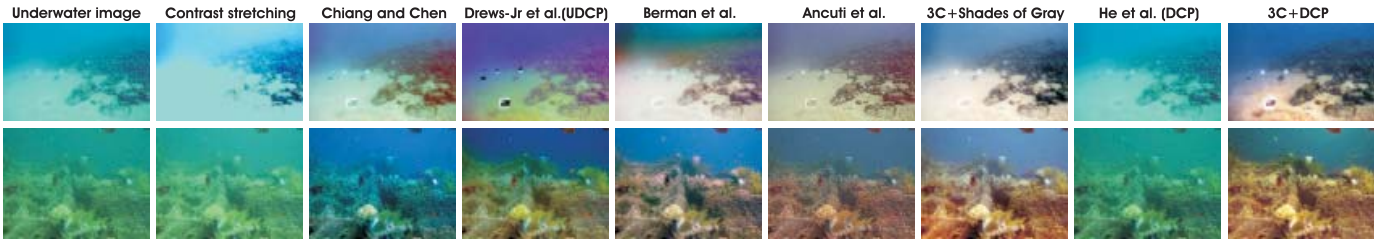

Fig. 15. **Underwater image enhancement.** Qualitative comparison of different specialized underwater dehazing approaches (Chiang and Chen [27], Drews-Jr et al. [10], Berman et al. [11], Ancuti et al. [12]) and the results of *Shades of Gray* [1] and DCP of images pre-processed by 3C operator.

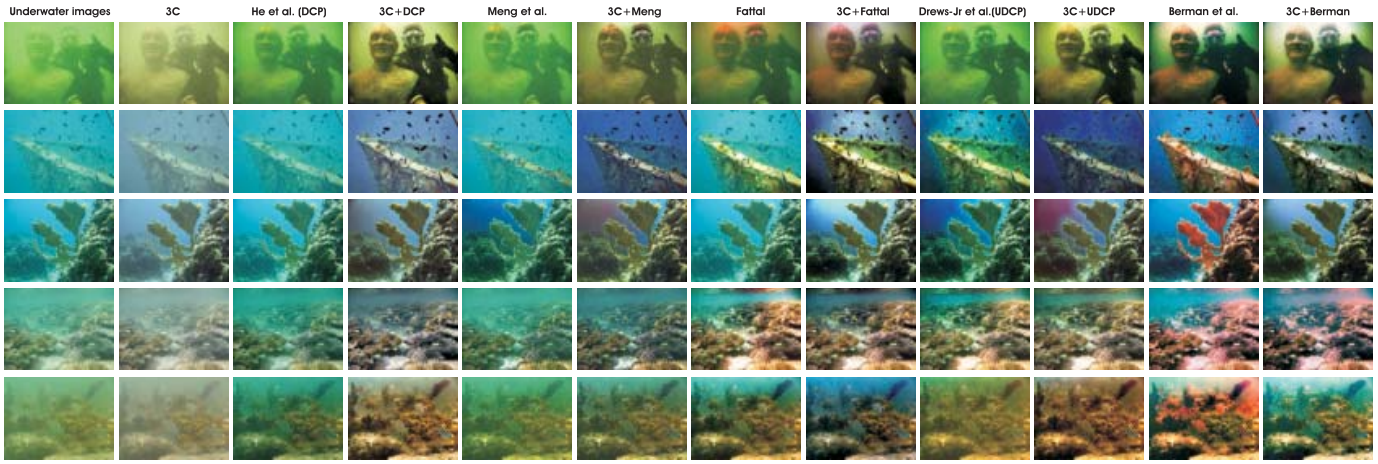

Fig. 16. **Underwater image enhancement.** Qualitative comparison of different image dehazing [2], [9], [16] and specialized underwater dehazing approaches (Drews-Jr et al. [10] and Berman et al. [11]) applied to images that have or have not been pre-processed with our 3C operator. The quantitative assessment of the entire set of 10 images presented in the supplementary material, are provided in Table V.

The volunteers were asked to rank the dehazed versions, presented in a random order, based on the restoration of color and details and taking into account the level of artifacts introduced. We used a set of 20 images (shown in the supplementary material and three examples are shown in Figure 13). The testing room was kept dark and the images were displayed using a calibrated 25 inch LED monitor (LG 25UM58-P, UltraWide Full HD). The participants were asked to rank the best four dehazed results. A score of 80%, 60%, 40% and 20% was assigned to those four images while the rest of them were classified as acceptable (scored with 10%) or not acceptable (not scored). We interpreted the results statistically using analysis of variance (ANOVA) [47]. It clearly appears from the statistical analysis plotted in Figure 14 that our 3C operator improves the perception of conventional method, with the best results being obtained by 3C + Li *et al.* [8].

Underwater image enhancement Although built on the same simplified optical model [13], underwater image enhancement is more challenging than outdoor image dehazing. However, as demonstrated in [12], when the most attenuated color channel is properly compensated, transmission can be reliably estimated based on the DCP, in underwater scenes as well.

In our experiments we observed that the 3C operator not only helped in estimating the transmission, but also in improving both global and local dehazing techniques. Fig. 17 presents two underwater images and the results yielded by specialized global [2], [10] and local [11] back-scattering techniques. Applying our operator (3C) as a pre-processing step, improves the level of object visibility in the restored image considerably.

We also considered the underwater image dataset of Berman *et al.* [11]. Fig. 15 shows three images of this dataset processed by different specialized underwater dehazing methods (Chiang and Chen [27], Drews-Jr *et al.* [10], Berman *et al.* [11], Ancuti *et al.* [12]). As can be seen, *Shades of Gray* [1] and DCP applied to images pre-processed by our operator (3C) yield very competitive results.

Additionally we performed a qualitative evaluation using the set of 10 underwater images used in the previous underwater studies [12], [28]. Fig. 16 shows five of those images and compares the results of He et al. (DCP) [2], Meng *et al.* [9], Fattal [16], Drews-Jr et al. (UDCP) [10], Berman *et al.* [11] with and without 3C pre-processing. The values of the PCQI [48] and UCIQE [49] metrics averaged over the entire set of images are shown in Table V. Again, 3C pre-processing helps to improve the image perception significantly. The absence of a ground-truth image (e.g., based on the inclusion of a color checker in the scene), however, prevents us from drawing definitive conclusions about color recovery.

C. Implementation and Limitations

Our technique is straightforward to implement. Its computational time is dominated by the (Gausian) filtering and

TABLE V

QUANTITATIVE EVALUATION OF UNDERWATER. PCQI [48] AND UCIQE [49] ARE AVERAGED OVER 10 IMAGES THAT ARE COMMONLY USED TO ASSESS UNDERWATER DEHAZING IN THE PREVIOUS UNDERWATER STUDIES [12], [28]. IMAGE DEHAZING HAS BEEN CONSIDERED WITH AND WITHOUT 3C PRE-PROCESSING. TESTED DEHAZING METHODS INCLUDE HE ET AL. (DCP) [2], MENG ET AL. [9], FATTAL [16], UDCP [10] AND BERMAN ET AL. [11]. FIVE IMAGES SAMPLES ARE SHOWN IN FIG. 16. THE READER IS REFERRED TO THE SUPPLEMENTARY MATERIAL FOR THE COMPLETE SET OF IMAGES AND COMPARATIVE RESULTS

	3C	**DCP** [2]	**3C+DCP**	**Meng** [9]	**3C+Meng**	**Fattal** [16]	**3C+Fattal**	**UDCP** [10]	**3C+UDCP**	**Berman** [11]	**3C+Berman**
PCQI	0.927	0.945	1.177	1.011	1.035	1.065	1.092	1.031	1.047	0.931	0.945
UCIQE	0.485	0.562	0.622	0.544	0.577	0.646	0.658	0.603	0.633	0.696	0.689

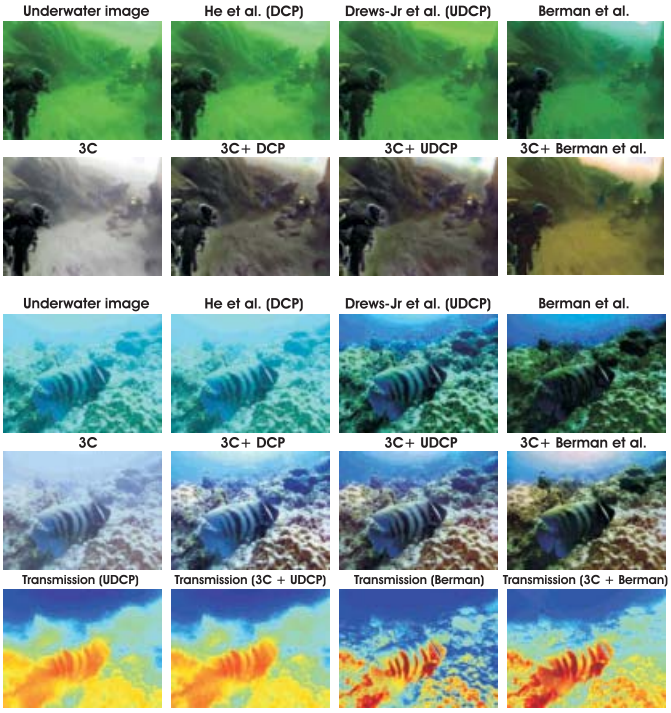

Fig. 17. **Underwater image enhancement.** Applying 3C as a pre-processing step for both global [2], [10] and local [11] back-scattering techniques largely improves the images. Interestingly, the bottom row demonstrates that even if transmission is relatively well estimated, this may not always help the methods of Berman et al. [11] and Drews-Jr et al. (UDCP) [10] to restore the visibility of underwater scenes.

TABLE VI

EXECUTION TIME OF OUR NON-OPTIMISED IMPLEMENTATION AS A FUNCTION OF THE IMAGE SIZE

Img. Resolution	480x720	960x1440	1440x2160	1920x2880	2400x3600	2880x4320	3360x5040
Exec. Time (s)	0.4535	0.8316	1.7748	3.0578	4.8372	6.9017	9.3639

the color space conversion (from RGB to CIELAB and vice-versa). TableVI provides the execution time of this non-optimized implementation[1] as a function of the image size, on a Intel Core i7, 16GB RAM.

While our approach exhibits impressive robustness, we have found that the main limitation of 3C appears in cases where the captured scenes contain regions for which two color channels are highly attenuated. For instance, in the image example shown in Fig. 18, only the red channel contains important information. While some of the color cast is removed by 3C, part of the color spectrum is lost and cannot be restored.

[1]The code of the 3C operator is released on the project page https://sites.uclouvain.be/ispgroup/Research/3C

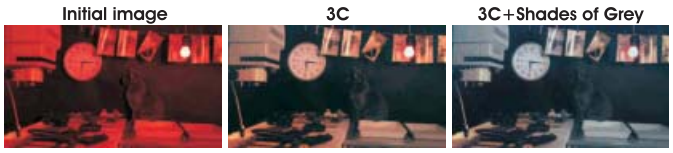

Fig. 18. **Limitations.** When the captured scenes contain regions with two color channels entirely attenuated, 3C performs poorly to restore the entire color spectrum.

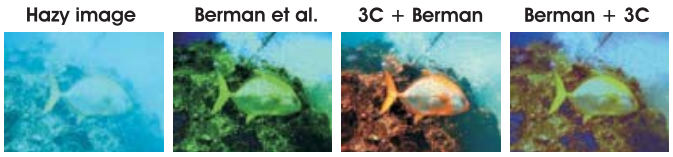

Fig. 19. **Applying 3C as pre-processing vs. post-processing.** Our operator 3C is more effective as a pre-processing than a post-processing operator.

Moreover, applying our 3C operator as a pre-processing step on the captured image is more beneficial in general than applying it as a post-processing operator (please refer to Fig. 19).

V. CONCLUSION

We introduced a novel operator (3C) to overcome artifacts resulting from the wavelength-specific scenes color attenuation encountered under night-time hazy conditions, in underwater images, or under artificial illumination. Our operator builds on the observation that opponent colors average to zero on large spatial neighborhoods, and has shown high robustness to enhance challenging scenes in which one color channel has been highly attenuated. Unlike to color constancy techniques, our 3C operator, focuses on compensating for the loss of one particular color channel (e.g., due to a selective illumination spectrum or strong attenuation of a subset of wavelengths). The lost color channel information is partly recovered by pushing the opponent colors towards a zero local mean. Despite its simplicity, 3C employed as a pre-processing step, consistently improves the outcome of conventional restoration processes. To prove the utility of 3C, we have provided an extensive qualitative and quantitative evaluation of several challenging enhancement applications, including color constancy, day-time and night-time image dehazing, and underwater enhancement.

REFERENCES

[1] G. D. Finlayson and E. Trezzi, "Shades of gray and colour constancy," in *Proc. 12th Color Imag. Conf. Final Program*, 2004, pp. 37–41.

[2] K. He, J. Sun, and X. Tang, "Single image haze removal using dark channel prior," in *Proc. CVPR*, Dec. 2009, pp. 2341–2353.

[3] G. Buchsbaum, "A spatial processor model for object colour perception," *J. Franklin Inst.*, vol. 310, no. 1, pp. 1–26, 1980.

[4] E. H. Land, "The retinex theory of color vision," *Sci. Amer.*, vol. 237, no. 6, pp. 108–129, 1977.

[5] J. van de Weijer, T. Gevers, and A. Gijsenij, "Edge-based color constancy," *IEEE Trans. Image Process.*, vol. 16, no. 9, pp. 2207–2214, Sep. 2007.

[6] Q. Zhu, J. Mai, and L. Shao, "A fast single image haze removal algorithm using color attenuation prior," *IEEE Trans. Image Process.*, vol. 24, no. 11, pp. 3522–3533, Nov. 2015.

[7] D. Berman, T. Treibitz, and S. Avidan, "Non-local image dehazing," in *Proc. CVPR*, Jun. 2016, pp. 1674–1682.

[8] Y. Li, R. T. Tan, and M. S. Brown, "Nighttime haze removal with glow and multiple light colors," in *Proc. ICCV*, Dec. 2015, pp. 226–234.

[9] G. Meng, Y. Wang, J. Duan, S. Xiang, and C. Pan, "Efficient image dehazing with boundary constraint and contextual regularization," in *Proc. ICCV*, Dec. 2013, pp. 617–624.

[10] P. Drews, Jr., E. Nascimento, S. Botelho, and M. F. M. Campos, "Underwater depth estimation and image restoration based on single images," *IEEE Comput. Graph. Appl.*, vol. 36, no. 2, pp. 24–35, Mar./Apr. 2016.

[11] D. Berman, T. Treibitz, and S. Avidan, "Diving into haze-lines: Color restoration of underwater images," in *Proc. BMVC*, 2017, pp. 1–12.

[12] C. O. Ancuti, C. Ancuti, C. De Vleeschouwer, and P. Bekaert, "Color balance and fusion for underwater image enhancement," *IEEE Trans. Image Process.*, vol. 27, no. 1, pp. 379–393, Jan. 2018.

[13] H. Koschmieder, "Theorie der horizontalen sichtweite," in *Beitrage Zur Physik Der Freien Atmosphare*, vol. 12. Leipzig, Germany: Akademie Verlagsges-Ellschaft Becker & Erler Kom.-Ges, 1924, pp. 171–181.

[14] R. T. Tan, "Visibility in bad weather from a single image," in *Proc. CVPR*, Jun. 2008, pp. 1–8.

[15] J.-P. Tarel and N. Hautière, "Fast visibility restoration from a single color or gray level image," in *Proc. ICCV*, Sep./Oct. 2009, pp. 2201–2208.

[16] R. Fattal, "Dehazing using color-lines," *ACM Trans. Graph.*, vol. 34, no. 1, p. 13, Nov. 2014.

[17] A. Galdran, A. Alvarez-Gila, A. Bria, J. Vazquez-Corral, and M. Bertalmío, "On the duality between retinex and image dehazing," in *Proc. CVPR*, Jun. 2018, pp. 8212–8221.

[18] C. O. Ancuti, C. Ancuti, C. De Vleeschouwer, and A. C. Bovik, "Single-scale fusion: An effective approach to merging images," *IEEE Trans. Image Process.*, vol. 26, no. 1, pp. 65–78, Jan. 2017.

[19] C. O. Ancuti and C. Ancuti, "Single image dehazing by multi-scale fusion," *IEEE Trans. Image Process.*, vol. 22, no. 8, pp. 3271–3282, Aug. 2013.

[20] L. K. Choi, J. You, and A. C. Bovik, "Referenceless prediction of perceptual fog density and perceptual image defogging," *IEEE Trans. Image Process.*, vol. 24, no. 11, pp. 3888–3901, Nov. 2015.

[21] C. Ancuti, C. O. Ancuti, A. C. Bovik, and C. De Vleeschouwer, "Night-time dehazing by fusion," in *Proc. IEEE Int. Conf. Image Process.*, Sep. 2016, pp. 2256–2260.

[22] K. Tang, J. Yang, and J. Wang, "Investigating haze-relevant features in a learning framework for image dehazing," in *Proc. CVPR*, Jun. 2009, pp. 2995–3000.

[23] B. Cai, X. Xu, K. Jia, C. Qing, and D. Tao, "DehazeNet: An end-to-end system for single image haze removal," *IEEE Trans. Image Process.*, vol. 25, no. 11, pp. 5187–5198, Nov. 2016.

[24] W. Ren, S. Liu, H. Zhang, J. Pan, X. Cao, and M.-H. Yang, "Single image dehazing via multi-scale convolutional neural networks," in *Proc. Eur. Conf. Comput. Vis.*, 2016, pp. 154–169.

[25] S.-C. Pei and T.-Y. Lee, "Nighttime haze removal using color transfer pre-processing and dark channel prior," in *Proc. 19th IEEE Int. Conf. Image Process.*, Sep./Oct. 2012, pp. 957–960.

[26] J. Zhang, Y. Cao, and Z. Wang, "Nighttime haze removal based on a new imaging model," in *Proc. IEEE Int. Conf. Image Process.*, Oct. 2014, pp. 4557–4561.

[27] J. Y. Chiang and Y. Chen, "Underwater image enhancement by wavelength compensation and dehazing," *IEEE Trans. Image Process.*, vol. 21, no. 4, pp. 1756–1769, Apr. 2012.

[28] S. Emberton, L. Chittka, and A. Cavallaro, "Hierarchical rank-based veiling light estimation for underwater dehazing," in *Proc. BMVC*, 2015, pp. 1–12.

[29] C. Ancuti, C. O. Ancuti, C. De Vleeschouwer, R. Garcia, and A. C. Bovik, "Multi-scale underwater descattering," in *Proc. 23rd Int. Conf. Pattern Recognit.*, Dec. 2016, pp. 4202–4207.

[30] C. O. Ancuti, C. Ancuti, C. De Vleeschouwer, L. Neumann, and R. Garcia, "Color transfer for underwater dehazing and depth estimation," in *Proc. IEEE Int. Conf. Image Process.*, Sep. 2017, pp. 695–699.

[31] C. O. Ancuti, C. Ancuti, C. De Vleeschouwer, and R. Garcia, "Locally adaptive color correction for underwater image dehazing and matching," in *Proc. CVPR*, Jul. 2017, pp. 1–9.

[32] A. Galdran, D. Pardo, A. Picón, and A. Alvarez-Gila, "Automatic red-channel underwater image restoration," *J. Vis. Commun. Image Represent.*, vol. 26, pp. 132–145, Jan. 2015.

[33] A. Gijsenij, T. Gevers, and J. van de Weijer, "Computational color constancy: Survey and experiments," *IEEE Trans. Image Process.*, vol. 20, no. 9, pp. 2475–2489, Sep. 2011.

[34] P. V. Gehler, C. Rother, A. Blake, T. Minka, and T. Sharp, "Bayesian color constancy revisited," in *Proc. CVPR*, Jun. 2008, pp. 1–8.

[35] A. Gijsenij and T. Gevers, "Color constancy using natural image statistics and scene semantics," *IEEE Trans. Pattern Anal. Mach. Intell.*, vol. 33, no. 4, pp. 687–698, Apr. 2011.

[36] S. Beigpour, C. Riess, J. van de Weijer, and E. Angelopoulou, "Multi-illuminant estimation with conditional random fields," *IEEE Trans. Image Process.*, vol. 23, no. 1, pp. 83–96, Jan. 2014.

[37] D. Cheng, B. Price, S. Cohen, and M. S. Brown, "Effective learning-based illuminant estimation using simple features," in *Proc. CVPR*, Jun. 2015, pp. 1000–1008.

[38] E. Hsu, T. Mertens, S. Paris, S. Avidan, and F. Durand, "Light mixture estimation for spatially varying white balance," *ACM Trans. Graph.*, vol. 27, no. 3, p. 70, 2008.

[39] A. Gijsenij, R. Lu, and T. Gevers, "Color constancy for multiple light sources," *IEEE Trans. Image Process.*, vol. 21, no. 2, pp. 697–707, Feb. 2012.

[40] D. Cheng, B. Price, S. Cohen, and M. S. Brown, "Two illuminant estimation and user correction preference," in *Proc. CVPR*, Jun. 2016, pp. 469–477.

[41] H. C. Karaimer and M. S. Brown, "Improving color reproduction accuracy on cameras," in *Proc. CVPR*, Jun. 2018, pp. 6440–6449.

[42] D. Mark Fairchild, *Color Appearance Models*, 2nd ed. Hoboken, NJ, USA: Wiley, 2005.

[43] S. Gould, R. Fulton, and D. Koller, "Decomposing a scene into geometric and semantically consistent regions," in *Proc. ICCV*, Sep./Oct. 2009, pp. 1–8.

[44] A. Gijsenij, T. Gevers, and J. van de Weijer, "Improving color constancy by photometric edge weighting," *IEEE Trans. Pattern Anal. Mach. Intell.*, vol. 34, no. 5, pp. 918–929, May 2012.

[45] G. Sharma, W. Wu, and E. Dalal, "The CIEDE2000 color-difference formula: Implementation notes, supplementary test data, and mathematical observations," *Color Res. Appl.*, vol. 30, no. 1, pp. 21–30, 2005.

[46] C. O. Ancuti, C. Ancuti, R. Timofte, and C. De Vleeschouwer, "O-HAZE: A dehazing benchmark with real hazy and haze-free outdoor images," in *Proc. CVPR*, Jun. 2018, pp. 754–762.

[47] B. G. Tabachnick and L. S. Fidell, *Using Multivariate Statistics*, 5th ed. Boston, MA, USA: Allyn & Bacon, 2005.

[48] S. Wang, K. Ma, H. Yeganeh, Z. Wang, and W. Lin, "A patch-structure representation method for quality assessment of contrast changed images," *IEEE Signal Process. Lett.*, vol. 22, no. 12, pp. 2387–2390, Dec. 2015.

[49] M. Yang and A. Sowmya, "An underwater color image quality evaluation metric," *IEEE Trans. Image Process.*, vol. 24, no. 12, pp. 6062–6071, Dec. 2015.

Codruta O. Ancuti received the Ph.D. degree from Hasselt University, Belgium, in 2011. From 2015 to 2017, she was a Research Fellow with ViCOROB Group, University of Girona, Spain. She is currently a Senior Researcher/Lecturer with the Faculty of Electrical and Telecommunication Engineering, Universitatea Politehnica Timisoara. Her main research interest includes image understanding and visual perception. She is the first that introduced several single images-based enhancing techniques built on the multiscale fusion (e.g., color-to-grayscale, image dehazing, underwater image, and video restoration). She received the Best Paper Award at NTIRE 2017 (CVPR workshop).

Cosmin Ancuti received the Ph.D. degree from Hasselt University, Belgium, in 2009. He was a Post-Doctoral Fellow with IMINDS and the Intel Exascience Laboratory (IMEC), Leuven, Belgium, from 2010 to 2012, and a Research Fellow with the University Catholique of Louvain, Belgium, from 2015 to 2017. He is currently a Senior Researcher/Lecturer with Universitatea Politehnica Timisoara, Romania, and the Institute of Informatics and Applications, University of Girona, Spain. He is the author of over 50 articles published in international conference proceedings and journals and co-organizes the IEEE CVPR NTIRE workshop. His area of research interests include image and video enhancement techniques, computational photography, and low-level computer vision.

Christophe De Vleeschouwer was a Senior Research Engineer with IMEC from 1999 to 2000, a Postdoctoral Research Fellow with the University of California at Berkeley from 2001 to 2002, EPFL in 2004, and a Visiting Faculty with Carnegie Mellon University from 2014 to 2015. He is currently the Research Director with the Belgian NSF, and an Associate Professor with the ISP Group, Universite Catholique de Louvain, Belgium. He has coauthored over 35 journal articles or book chapters, and holds two patents. His main research interests include in video and image processing for content management, transmission, and interpretation. He is also enthusiastic about nonlinear and sparse signal expansion techniques, the ensemble of classifiers, multiview video processing, and the graph-based formalization of vision problems. He served as an Associate Editor for the IEEE TRANSACTIONS ON MULTIMEDIA, and has been a (Technical) Program Committee Member for most conferences dealing with video communication and image processing.

Mateu Sbert received the M.Sc. degree in physics from Valencia University, in 1977, the degree in mathematics from UNED, Madrid, in 1983, and the Ph.D. degree in computer science from Barcelona TU, in 1997. He is currently a Professor in computer science with Tianjin University, China, and the University of Girona, Spain. He has authored or coauthored more than 200 articles and four books, receiving more than 4000 citations to his work. His research interests include Monte Carlo, integral geometry and information theory techniques for computer graphics, and image processing and visualization. He received the Best Ph.D. Award from Barcelona TU.